Niğde Ömer Halisdemir Üniversitesi Mühendislik Bilimleri Dergisi
Nigde Omer Halisdemir University Journal of Engineering Sciences
ISSN: 2564-6605
Araştırma / Research

THE EVALUATION OF CORROSION BEHAVIOUR OF Al/Y_2O_3 NANO COMPOSITES BY POWDER METALLURGY AT ROOM AND ELEVATED TEMPERATURE

Fatih AYDIN[1*]

[1]*Department of Metallurgical and Materials Engineering, Karabuk University, Karabuk, TURKEY*

ABSTRACT

In this study, Al / Y_2O_3 metal matrix nanocomposites (2 and 4 wt. %) were fabricated by powder metallurgy route. The microstructure and density of the fabricated samples were investigated. Microstructure characterization shows that the homogenous distribution of particulates was achieved. Furthermore, the corrosion behaviour of the samples was systematically investigated in 1 M HCl solution by potentiodynamic and immersion tests for temperature of 20°C and 50 °C. In order to understand the corrosion mechanisms, SEM study was performed. The potentiodynamic corrosion test results show that Al / $4Y_2O_3$ composite has the best corrosion performance at room temperature. After the immersion tests, the weight loss of the composites has higher than that of pure Al at elevated temperature (50 ºC). Pitting and grain boundary corrosion were observed. The wear tests were performed for the samples under dry sliding conditions. The addition of Y_2O_3 particles give rise to significant increase in wear performance.

Keywords: Al matrix composites, Corrosion, Powder metallurgy, Microstructure

TOZ METALURJİSİ İLE ÜRETİLMİŞ Al / Y_2O_3 NANOKOMPOZİTLERİNİN ODA VE YÜKSEK SICAKLIKTAKİ KOROZYON DAVRANIŞININ İNCELENMESİ

ÖZET

Bu çalışmada, Al / Y_2O_3 metal matrisli nanokompozitleri (%2 ve %4 ağ.) toz metalurjisi ile üretilmiştir. Üretilen numunelerin mikroyapı ve yoğunlukları incelenmiştir. Mikroyapı karakterizasyonu partiküllerin homojen dağıldığını göstermiştir. Ayrıca, numunelerin korozyon davranışları, 20ºC ve 50ºC'de 1 M HCl çözeltisinde potansiyodinamik ve daldırma testleriyle sistematik olarak incelenmiştir. Korozyon mekanizmalarını anlamak için, SEM çalışması gerçekleştirilmiştir. Potansiyodinamik korozyon test sonuçları, Al / $4Y_2O_3$ kompozitinin oda sıcaklığında en iyi korozyon performansına sahip olduğunu göstermiştir. Daldırma testi sonunda, yüksek sıcaklıkta (50 ºC), kompozitlerin ağırlık kayıplarının saf Al'a göre fazla olduğu gözlenmiştir. Oyuklanma ve tane sınırı korozyonu gözlenmiştir. Numuneler için kuru kayma koşullarında aşınma testleri gerçekleştirilmiştir. Y_2O_3 partiküllerinin eklenmesi, aşınma performansında önemli bir artış sağlamıştır.

Anahtar kelimeler: Al matrisli kompozitler, Korozyon, Toz metalurjisi, Mikroyapı

1. INTRODUCTION

Aluminium metal matrix composites (Al-MMCs) have excellent properties such as high strength to weight ratio, stiffness, good machinability and high thermal conductivity [1]. These unique properties lead to large usage of Al-MMCs in aerospace, transportation and different industrial areas [2]. To reinforce the Al, different reinforcement particulates are commonly used such as SiC [3-5], Al_2O3 [6-9], B_4C [10-13], TiC, [14-17], ZrO_2 [18,19] CNT [20]. From the literature studies, it can be concluded the mechanical and wear behaviour of Al-MMCs are largely investigated. Corrosion is another important property which significantly affect the service life of Al-MMCs [21].While mechanical and wear properties are analysed, the investigation of corrosion behaviour is relatively limited.

Han et al. have examined the electrochemical corrosion behaviour of Al/B_4C composites in NaCl solution. The results of the study demonstrated that the corrosion rate of the Al increased with increasing B_4C content. The low corrosion resistance of the composites was attributed to galvanic couples between Al matrix and B_4C particles [22]. Zakaria has also examined the corrosion

* Sorumlu yazar / Corresponding author, e-posta / e-mail: fatih.aydin@karabuk.edu.tr
Geliş / Recieved: 14.03.2019 Kabul / Accepted: 21.11.2019 doi: 10.28948/ngumuh.539958

performance of Al-SiC composites in 3.5 wt. % NaCl solution by immersion tests for 25, 50 and 75°C. It was reported that Al/SiC composites had better corrosion resistance than that of pure Al at room temperature. However, at elevated temperatures, composites exhibited lower corrosion resistance [21].

Y_2O_3 is an another important candidate due to its thermal stability at elevated temperatures for reinforcement in Al-MMCs [23]. In one of those studies, Gonzalez-Rodriguez et al. have investigated the corrosion behaviour of Al-Mg-Zn-Si alloy and Al-Mg-Zn-Si / Y_2O_3 composite by electrochemical methods in 3.5 % NaCl solution. The specimens were produced by mechanical alloying and heat treated at 350 ˚C, 400 ˚C and 500 ˚C during 60 min followed by water quenching. It is reported that the corrosion resistance of alloy was higher than that of composite. However, heat-treated composite exhibits higher corrosion resistance among the samples. Pitting corrosion was observed after examination of corroded surfaces. It is concluded that matrix and Y_2O_3 particles acted as micro cathode and active anode, respectively [24].

To the best of our knowledge, no study was detected on corrosion behaviour of pure Al / Y_2O_3 composites in HCl solution for room and elevated temperatures by electrochemical and immersion tests. The aim of this study is to evaluate corrosion behaviour of Al/Y_2O_3 composites in 1 M HCl solution at room and elevated temperatures. Al/Y_2O_3 composites were manufactured by means of powder metallurgy with hot pressing. The effect of addition of Y_2O_3 on density, microstructure, wear and corrosion properties of Al were systematically investigated. In order to evaluate corrosion mechanisms, corroded surfaces were examined by Scanning Electron Microscopy.

2. EXPERIMENTAL STUDY

In this study, Al powder (purity, 99.5 %; particle size ~100 μm) and Y_2O_3 powder (particle size, ~50 nm) were used as matrix and reinforcement materials, respectively. Al - Y_2O_3 composites (2 and 4 wt. %) were produced by semi powder metallurgy including steps of ultrasonication and vacuum distillation. Firstly, nano-Y_2O_3 powders were ultrasonicated in ethanol for 3 hours so as to avoid agglomerations of powders. In second step, Al powder was poured to ethanol solution including Y_2O_3. Al/Y_2O_3 powders were mixed using mechanical stirrer. Ethanol was removed from the system after two hours. Lastly, mixed powders were dried at 200 °C under argon atmosphere to avoid oxidation.

Powders were pressed at 600 °C with pressure of 50 MPa by hot pressing machine (MSE, HP_1200). All productions were performed under argon atmosphere. The diameter and height of the specimens were about 15 mm and 22 mm, respectively. In order to measure the actual density of the samples, Radwag electronic balance was used.

For metallographic examination, specimens were ground with SiC emery papers followed by polishing with 6 and 3 μm diamond solution. Samples were etched with Keller solution in order to reveal grain boundaries. Microstructure characterization of the samples was performed by Scanning Electron Microscope (SEM, Carl Zeiss Ultra Plus) equipped with an energy dispersive spectrometer (EDS, Bruker X Flash 6/10). Also, phase analyzes were performed using XRD device equipped with a monochromator and Cu (Kα radiation, λ: 1.54A°) (Rigaku Ultima IV). The diffraction patterns were obtained for 2θ Bragg angles ranging between 10° and 90°. The scanning speed was 3° / min for the measurements.

Hardness measurements were performed with hardness device (Qness, Q10 A+) with load of 0.5 kg for 10s. The wear tests were performed by reciprocating wear tester (UTS, T10/20) under dry sliding conditions. The type of wear was metal-metal sliding wear. The counterface material with hardness of 62 HRC was chosen as AISI 52100 steel. The sliding distance was 200 m for wear tests. The wear test parameters were given in Table 1.

Table 1. Wear test parameters

Parameters	Values
Stroke, mm	8
Counterface material	AISI 52100 steel
Frequency, Hz	5
Sliding distance, m	200
Sliding speed, mm/s	80, 120
Load, N	5, 10, 20
Test temperature, °C	23±2

Figure 1 shows the image and schematic representation of wear test setup. In this system, wear tests were performed with ball-on-disc configuration. The ball and disc were counterface material and sample, respectively.

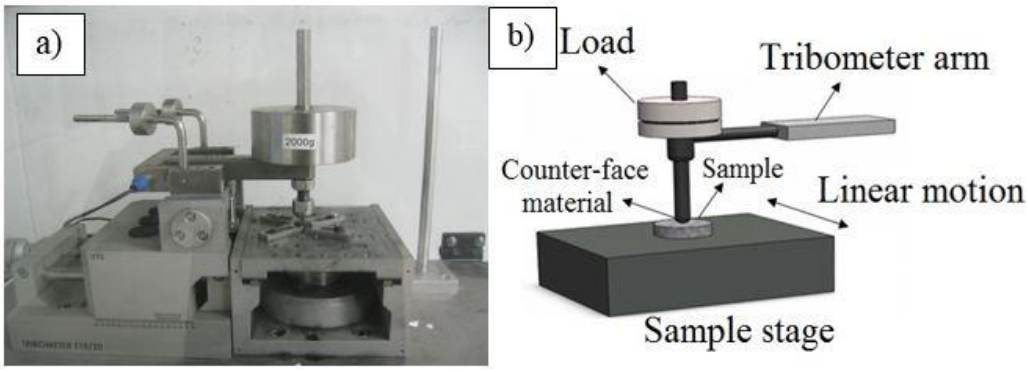

Figure 1. (a) The image and (b) schematic representation of wear test setup

To evaluate electrochemical corrosion performance of the samples, potentiodynamic polarization measurement was performed in 1 M HCl solution by using Parstat 4000 model potentiostat/galvanostat. $Ag/AgCl_2$ electrode was used as reference electrode. The interval of – 500 mV and 500 mV was used versus open circuit potentials (OPC). Scanning rate was determined as 1 mV/s. The electrochemical tests were performed at 20° C and 50 °C. Also, immersion test was carried out to support the results of electrochemical tests. Firstly, samples weighed before immersion test and later taken after 12 and 24 h, respectively. Corroded surfaces of the immersed samples were examined by SEM. Figure 2 shows the image of hot pressing system and corrosion test setup.

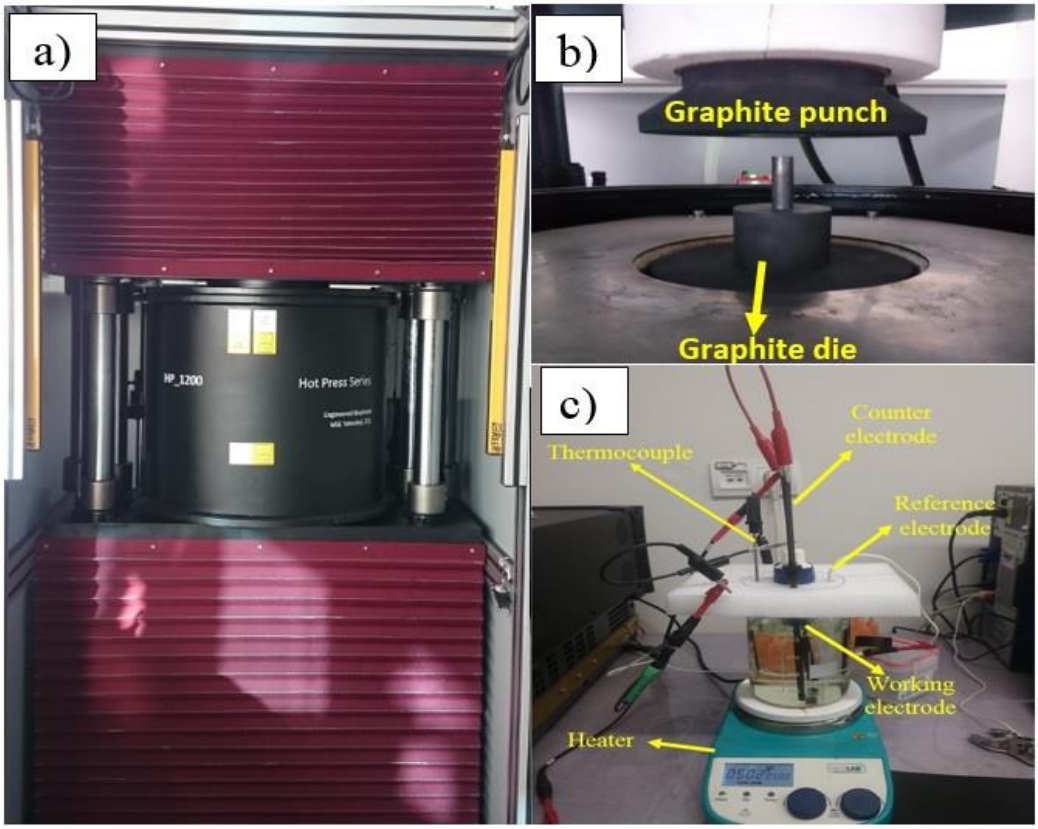

Figure 2. (a,b)The image of hot pressing system and (c) corrosion test setup.

3. RESULTS AND DISCUSSION

The theoretical, actual and relative density values of the samples are given in Table 2. As can be seen in Table 2, Al sample has the highest relative density (98.59 %). It is also clear that the relative density values of the composites were decreased with increasing reinforcement content. This can be attributed to the presence of micro-porosities in the structure of composite materials. The presence of micro-porosities are clearly seen in the microstructure of Al / $4Y_2O_3$ composite (Fig. 3c). The increase in micro-porosities and decrease in relative density with increasing reinforcement content is consistent with literature studies on metal matrix composites [25, 26]. From the Table 2, it is seen that hardness values of the samples increase with increasing Y_2O_3 content. The increase in hardness can be related to the presence of hard nano-Y_2O_3 particles and dispersion hardening effect. The hardness values of the samples are consistent with an another study in the literature [27].

Table 2. The density and hardness values of the samples

Materials	Theoretical density (g/cm^3)	Actual density (g/cm^3)	Relative density (%)	Hardness (HV)
Al	2.700	2.662±0.003	98.59	46±2.1
Al / $2Y_2O_3$	2.746	2.670±0.005	97.23	57±2.9
Al / $4Y_2O_3$	2.792	2.667±0.008	95.54	64±3.1

Figure 3 represents the SEM images of the samples. From the Fig. 3a, the grain boundaries of Al sample are clearly observed. For the composite materials, it can be seen that the nano-Y_2O_3 particles are located at the grain boundaries of the Al matrix. Also, the micro-porosities and agglomeration of nano-Y_2O_3 particles are observable for Al - $4Y_2O_3$ composite. Figure 4 shows the EDS analysis of Al- $2Y_2O_3$ composite. The EDS analysis of Al matrix (rectangle 1) showed significant amount of Al (98.91 %) and low amount of O (1.09 %). The very low content of O is mainly related to the realization of manufacturing process under argon atmosphere. At the EDS analysis of grain boundary of the sample, very high content of Y (66.37%) and O (27.66%) was detected. This is verified the presence of Y_2O_3 particulates in the structure of the composite.

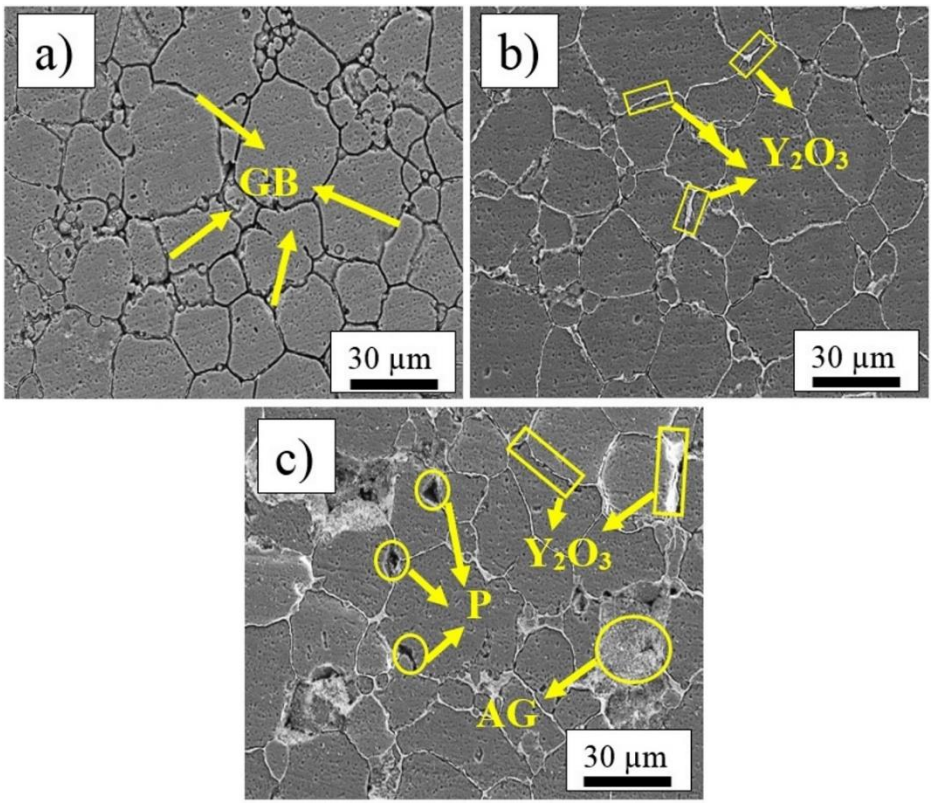

Figure 3. SEM images of a) pure Al, b) Al-$2Y_2O_3$ and c) Al-$4Y_2O_3$

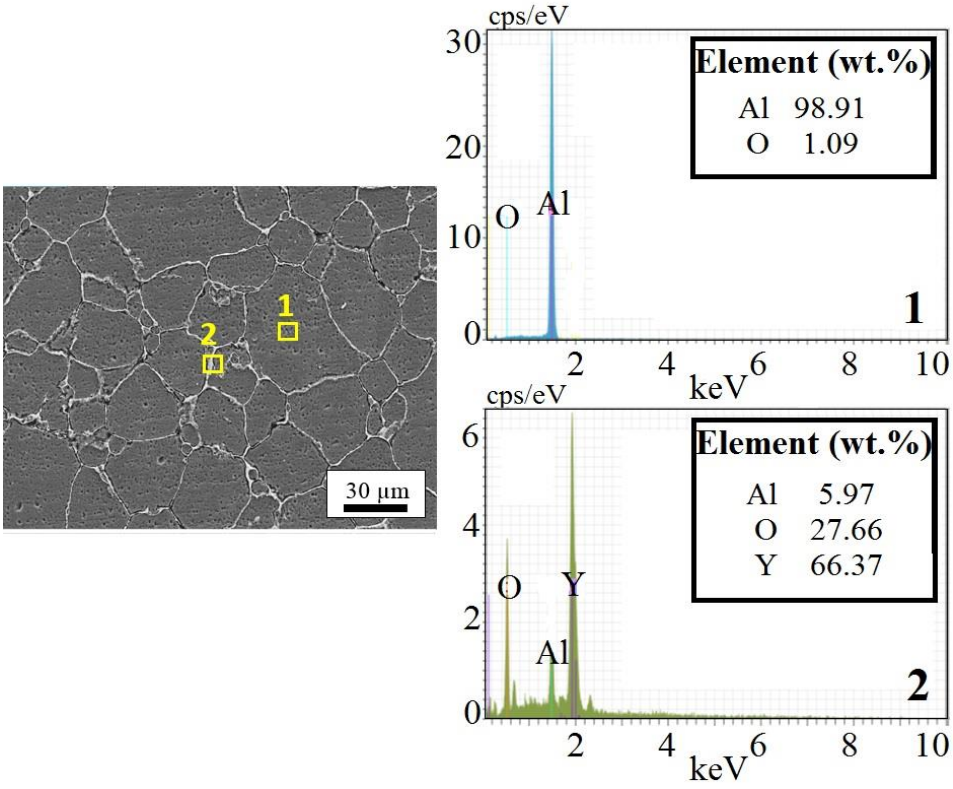

Figure 4. EDS analysis of Al-2Y_2O_3 composite

Figure 5 shows the XRD patterns of the samples. For pure Al sample, only Al diffraction peak from different crystallographic planes are detected. For the composite materials, both Al and Y_2O_3 diffraction peak are present in the structure. It is also said that there are no intermetallic phase and oxides between matrix and reinforcement. The intensity of the Y_2O_3 peaks increased with increasing Y_2O_3 content.

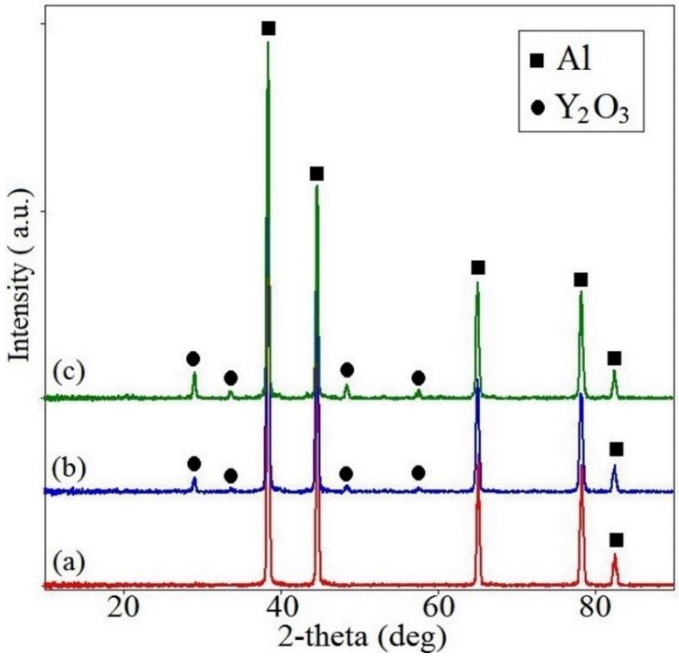

Figure 5. XRD patterns of the samples a) pure Al, b) Al-2Y_2O_3 and c) Al-4Y_2O_3

Figure 6 a-b shows the wear rate under load of 5N, 10N and 20N for sliding speed of 80 and 120 mm/s, respectively. It is seen that the addition of nano-Y_2O_3 particles leads to significant increase in wear resistance. For all loads, Al - $4Y_2O_3$ composite shows the best wear performance. The increase in wear resistance with increasing reinforcement content is related to the presence harder Y_2O_3 particles which leads to resistance to plastic deformation of matrix [28]. It is also seen that the wear rates of the samples shows mild increase with increasing sliding speed for composite materials. However, this increase is clear for pure Al sample. It is well known that sliding speed affects the frictional heat between counterface and sample. Generally, the frictional heat increases with increasing sliding speed. As the sliding speed increases, the sample is exposed to higher frictional heat. As a result, penetration of counter surface becomes severe, which give rise to higher wear rates [29].

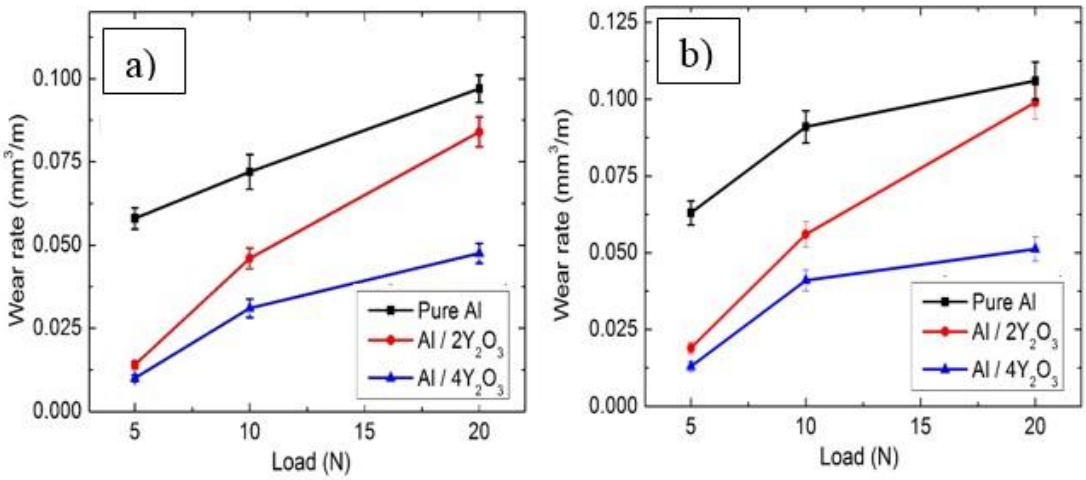

Figure 6. Wear rate graph for Al and Al matrix composites for different sliding speeds a) 80 mm/s and b) 120 mm/s

Figure 7 shows the worn surface images of the samples under load of 5 and 20 N for sliding speed of 80 mm/s. Fig. 7 a-b shows the presence of craters on the worn surface images of pure Al. From the transition 5 N to 20 N, the deep craters can be observed. The existence of craters verifies the presence of delamination wear [28]. For composite materials (Fig 7.c-d), the smooth surfaces can be clearly observed. Under load of 20 N, several cracks are present for Al- $4Y_2O_3$ composite. These cracks perpendicular to the sliding direction can be related to the existence of delamination wear [28].

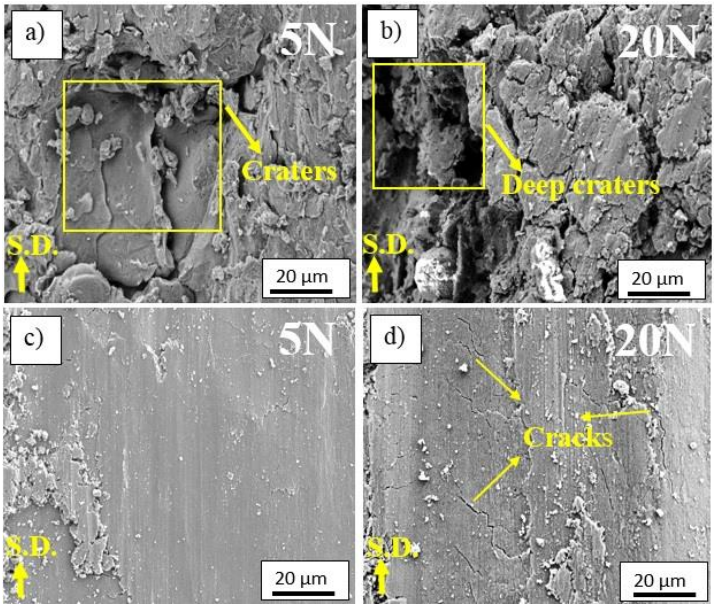

Figure 7. Worn surface images of the a-b) Al and c-d) Al-$4Y_2O_3$ under different loads for sliding speed of 80 mm/s (S.D. means sliding direction)

Figure 8 shows the worn surface images of the samples under load of 5 and 20 N for sliding speed of 120 mm/s. For pure Al, craters can be clearly observed. This is the result of delamination wear. For composite material under load of 5 N, grooves are present in the worn surface. The existence of grooves can be attributed to the presence of abrasive wear [28]. From the transition 5 N to 20 N, craters emerge in the structure of composite materials. It can be said that dominant wear mechanism is delamination.

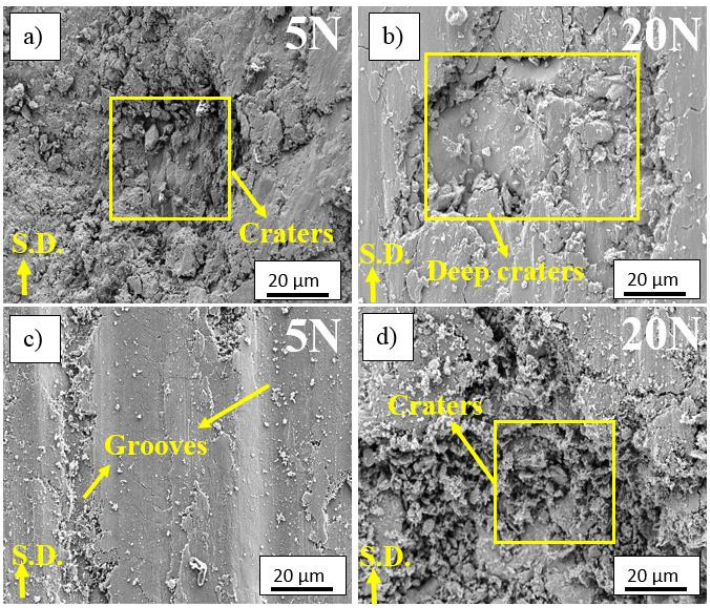

Figure 8. Worn surface images of the a-b) Al and c-d) Al-4Y_2O_3 under different loads for sliding speed of 120 mm/s (S.D. means sliding direction)

Figure 9 shows the potentiodynamic polarization curves of the samples at 20 and 50 ºC. The corrosion potentials, corrosion current densities and corrosion rates are calculated using Tafel extrapolation. The corrosion results of the samples are given in Table 2. The corrosion rate of the samples was calculated using equation 1 [30]:

$$\text{Corrosion rate (mm/year)} = \lambda . i_{corr} . (\text{E.W.}) / d \qquad (1)$$

Where;
$\lambda = 3.27 \times 10^{-3}$ (mm. g) / (mA. cm. year) is a metric conversion factor
i_{corr}= Corrosion rate (mA)
E.W=Equivalent Weight
d=Density (g/cm^3)

As can be seen in Table 3, firstly, the corrosion rate was increased for 2 wt. % Y_2O_3 reinforcement and considerably dropped for 4 wt. % Y_2O_3 at 20°C. Also, the samples have the similar behaviour at 50°C. The increase in test temperature led to increase in corrosion rate for all samples. However, this increase is drastic especially for composite materials. In the literature, the effect of temperature on the corrosion rate was depended on two factors: temperature variation of corrosion gradient and the energy of activation of corrosion. Corrosion rates can be significantly increased with activation energy owing to the increase in permeation rate [31].

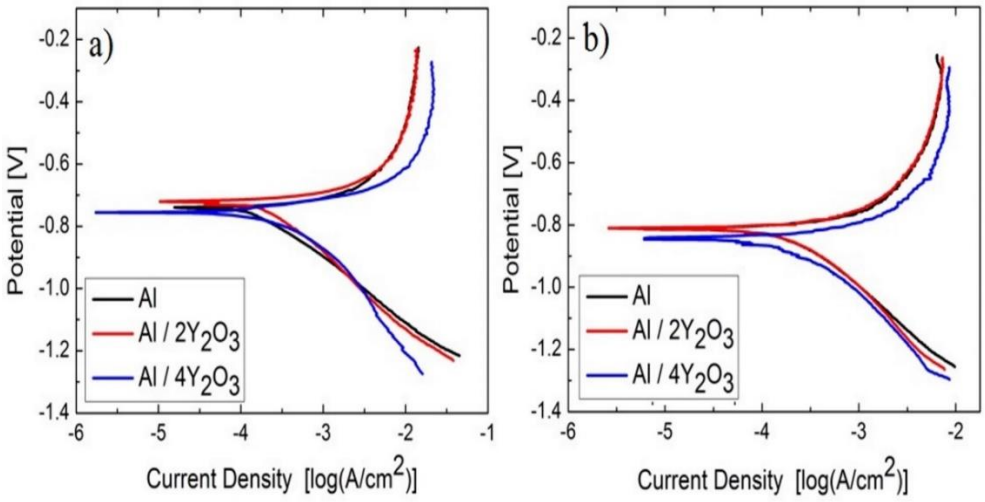

Figure 9. Potentiodynamic curves of the samples a) 20 °C and b) 50 °C

Table 3. Corrosion results of the samples.

Materials	E_{corr} (mV)	i_{corr} (µA)	CR (mm/year)
Al (20°C)	-729.04	309.18	1.93
Al / $2Y_2O_3$ (20°C)	-733.08	399.67	2.56
Al / $4Y_2O_3$ (20°C)	-751.76	254.11	1.69
Al (50°C)	-814.58	311.90	1.94
Al / $2Y_2O_3$ (50°C)	-817.39	456.88	2.93
Al / $4Y_2O_3$ (50°C)	-848.91	303.98	2.02

Figure 10 shows the weight loss change of the samples versus different time and Y_2O_3 content at 20 ºC and 50 ºC. As can be seen in Fig. 8a, pure Al has the highest weight loss for both 12 h and 24 h at 20 ºC in comparison with composite materials. Also, it is observed that increasing Y_2O_3 content led to significant decrease in weight loss. The reason of decrease in weight loss for composites at room temperature is attributed to the presence ceramic particulates in the structure which remain inert in the solution [21]. However, at 50 ºC, the weight loss of the samples increased with increasing reinforcement content for 12 h and 24 h. It is also worth to say that Al-$2Y_2O_3$ composite exhibits the worst corrosion performance for long term condition (24h).

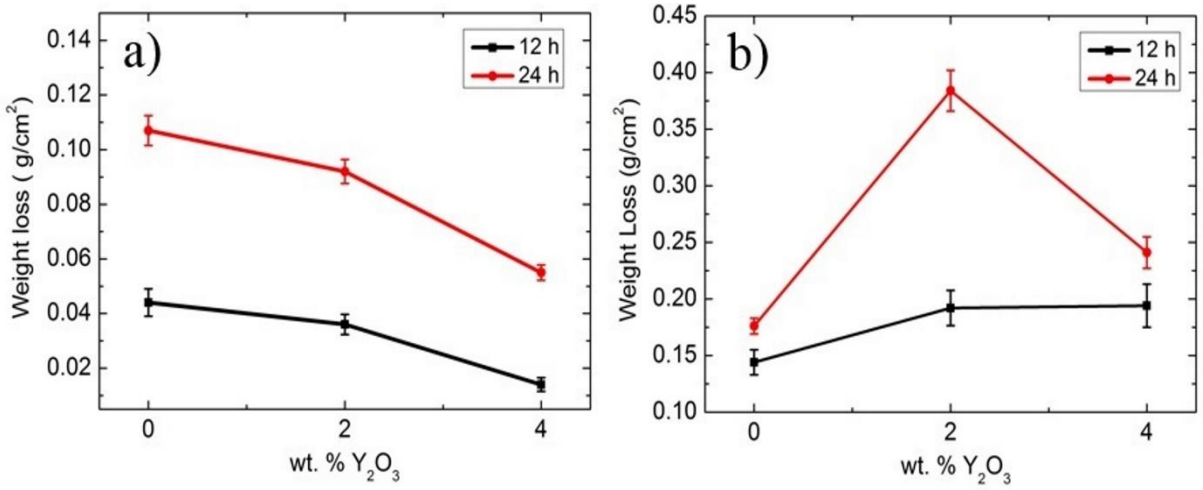

Figure 10. Weight loss change of the samples versus different time and Y_2O_3 content a) 20 ºC and b) 50 ºC.

The percentages of weight loss of the samples were given in Table 4. It is clearly seen that the percentages of weight loss are consistent with the weight loss of the samples. Al / $4Y_2O_3$ sample shows the lowest percentage of weight loss both for 12 h and 24 h at 20 °C. However, the percentages of weight loss of the samples increased with increasing Y_2O_3 content for 12 h at 50 °C.

Table 4. The percentages of weight loss of the samples (%).

	20°C		50°C	
Materials	**12h**	**24h**	**12h**	**24h**
Al	23.1	39.3	57.1	66.5
Al / $2Y_2O_3$	21.0	36.1	71.3	87.2
Al / $4Y_2O_3$	19.7	32.1	73.1	76.3

Figure 11 shows the SEM micrographs of the corroded samples at 20 ºC for 12 h. Some cracks are observed for pure Al, which can act as crevices where localized corrosion can occur [24]. For the composite materials, the grain boundary corrosion and pitting corrosion were identified as corrosion mechanisms. Zakaria et al. have reported the presence of pitting and grain boundary corrosion for Al/SiC composites [21]. The pitting corrosion can be occurred at the sites where the Y_2O_3 particulates agglomerate.

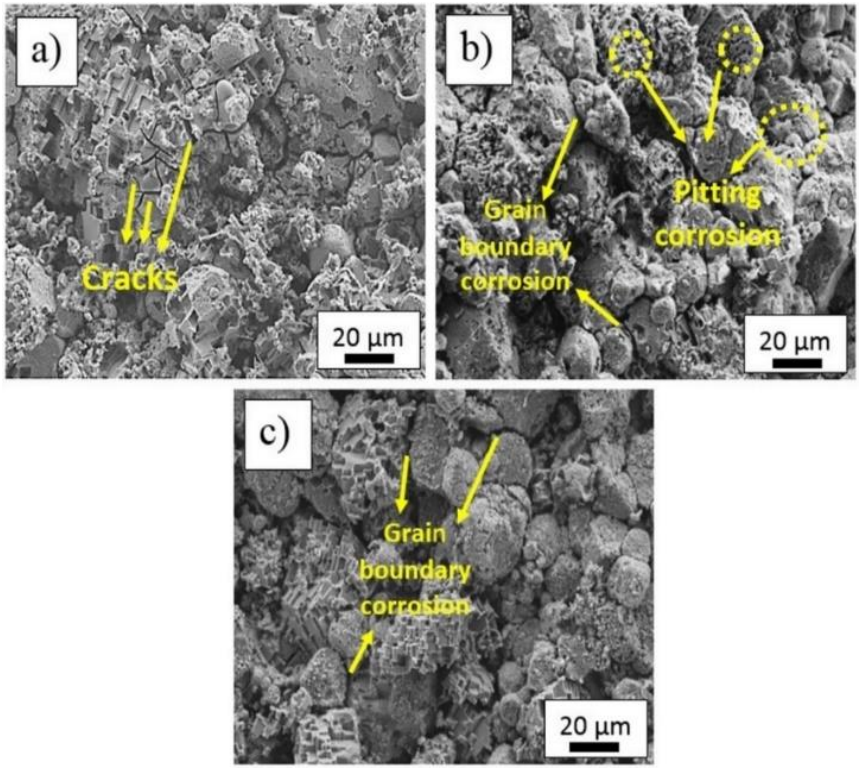

Figure 11. SEM micrographs of the corroded samples at 20 ºC for 12 h: a) pure Al, b) Al-$2Y_2O_3$ and c) Al-$4Y_2O_3$

Figure 12 shows the EDS analysis of samples after immersed for 12 h at 20 ºC. It is worth to say that high O content (12.8) and Cl content (1.0) was detected on the analysis of the cracks for pure Al (rectangle 2). This results confirms that the formation of aluminium oxide after immersion test. For Al-$4Y_2O_3$ composite, the EDS analysis of rectangle 2 shows the high significant amount of O (27.4) and low amount of Y (1.6). The presence of Y after immersion tests shows that the Y2O3 particles resist to propagation of corrosion.

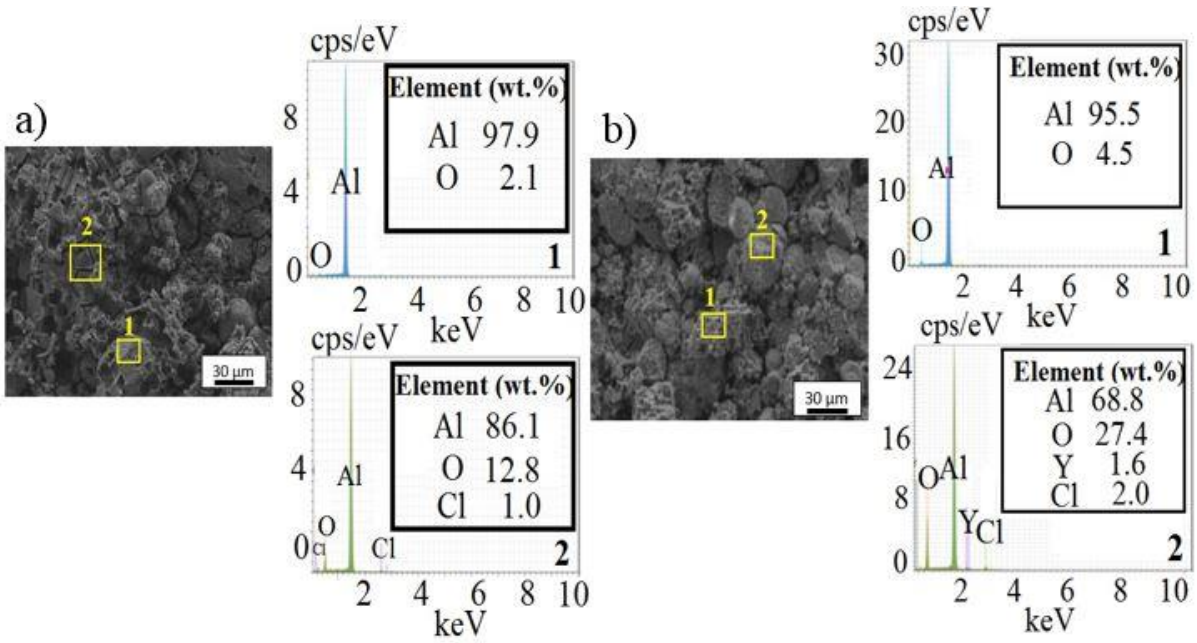

Figure 12. EDS analysis of a) pure Al and b) Al-4Y_2O_3 after immersed for 12 h at 20 ºC.

Figure 13 shows the SEM micrographs of the corroded samples at 50 ºC for 12 h. For pure Al, deep cracks are observed on the image of the corroded surface. It is clear from the figures that severe degradation along grain boundaries was clearly seen for composite materials. It is concluded that the increase in test temperature (from 20 ºC to 50 ºC) give rise to significant deterioration for the composite materials. It is reported that severity of damage in the Al-MMCs increases with increasing exposure duration and test temperature [21].

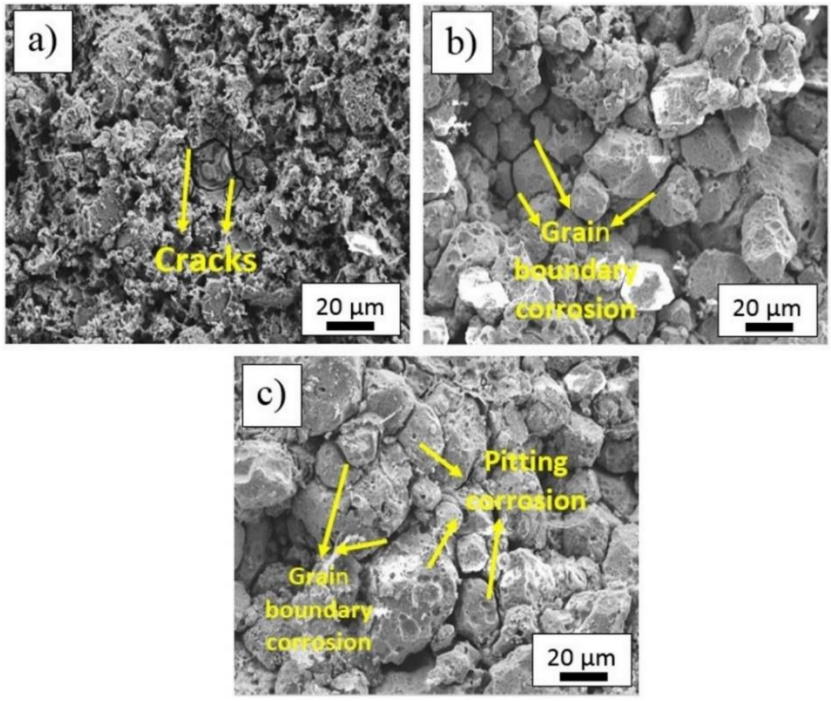

Figure 13. SEM micrographs of the corroded samples at 50 ºC for 12h: a) pure Al, b) Al-2Y_2O_3 and c) Al-4Y_2O_3

Figure 14 shows the EDS analysis of samples after immersed for 12 h at 50 ºC. The EDS analysis of area 1 shows the only Al (82%) and O (18%), indicating the presence of only aluminium and aluminium oxide. Also, significant amount of Al, O and Cl was detected for the EDS analysis of area 2. It can be said that Cl comes from HCl solution. The EDS analyses of Al-4Y2O3 verifies the presence aluminium oxide and yttrium oxide in the structure of immersed surface.

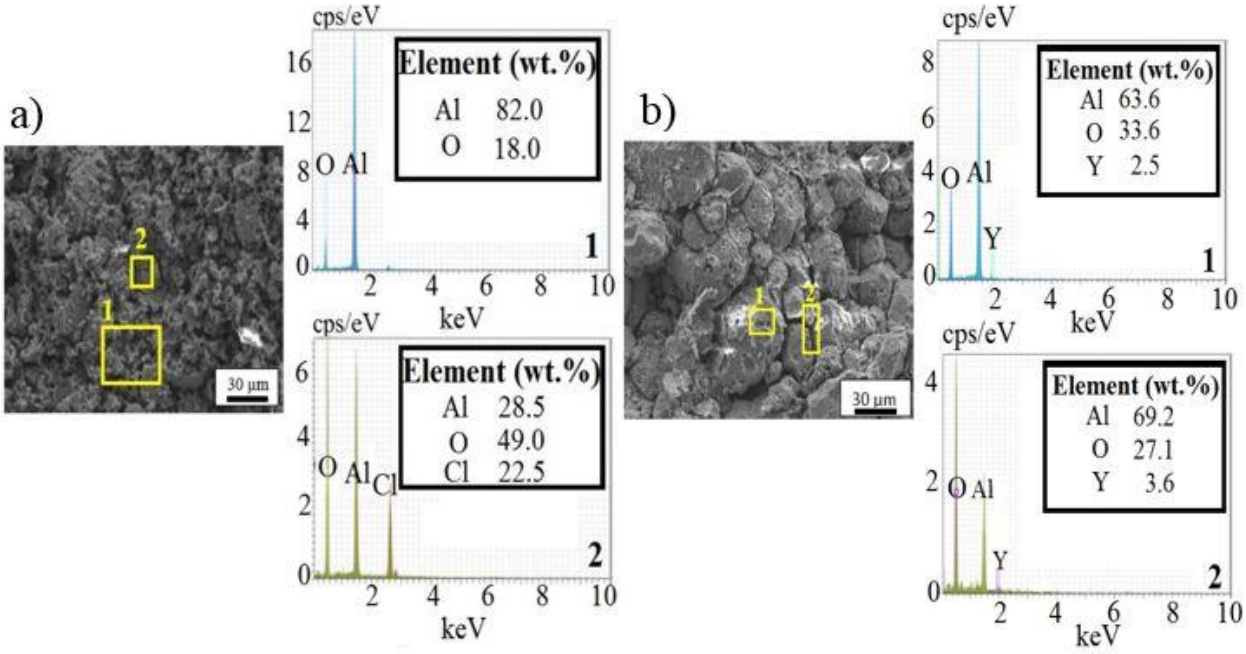

Figure 14. EDS analysis of a) pure Al b) and Al-4Y_2O_3 after immersed for 12 h at 50 ºC.

4. CONCLUSIONS

In this study, Al and Al / Y_2O_3 nanocomposites (2 and 4 wt. %) were successfully fabricated by powder metallurgy route using hot pressing. The following results can be pointed out:

- The actual density values of the samples decreased with increasing reinforcement content.
- The homogenous distribution of particulates was achieved. However, agglomeration of particulates was seen with increasing reinforcement content.
- The presence of Al and Y_2O_3 was verified by XRD analysis.
- Potentiodynamic corrosion tests show that Al / 4Y_2O_3 composite has the best corroison performance at room temperature. However, at the temperature of 50 ºC, pure Al exhibits the lower corrosion rate among the samples.
- Immersion tests show that weight loss of the samples decrease with increasing reinforcement content for 12 h and 24 h at room temperature. The increase in test temperature leads to considerable increase in weight loss of the composite samples.
- The pitting and grain boundary corrosion were determined as general corrosion mechanisms for samples.
- The wear rate of the samples decreased with increasing Y_2O_3 content.

REFERENCES

[1] S. Soltani, R. A. Khosroshahi, R. T. Mousavian, Z. Y. Jiang, A. F. Boostani and D. Brabazon, “Stir casting process for manufacture of Al–SiC composites,” Rare Metals, vol. 36, no. 7, pp. 581-590, 2017.

[2] B. V. Ramnath, C. Elanchezhian, R. M. Annamalai, S., Aravind, T. S. A. Atreya, V, Vignesh and C. Subramanian, “Aluminium metal matrix composites - a review,” Reviews On Advanced Materials Science, vol. 38, pp. 55-60, 2014.

[3] H. Izadi, A. Nolting, C. Munro, D. P. Bishop, K. P. Plucknett and A. P. Gerlich, "Friction stir processing of Al/SiC composites fabricated by powder metallurgy," Journal of Materials Processing Technology, vol. 213, no. 11, pp. 1900-1907, 2013.

[4] F. Teng, K. Yu, J. Luo, H. Fang, C. Shi, Y. Dai and H. Xiong, "Microstructures and properties of Al−50%SiC composites for electronic packaging applications," Transactions of Nonferrous Metals Society of China, vol. 26, no. 10, pp. 2647-2652, 2016.

[5] L. Zhang, H. Xu, Z. Wang, Q. Li and J. Wu, "Mechanical properties and corrosion behavior of al/sic composites", Journal of Alloys and Compounds, vol. 678, pp. 23-30, 2016.

[6] S. M. Zebarjad and S. A. Sajjadi, "Microstructure evaluation of Al–Al_2O_3 composite produced by mechanical alloying method," Materials and Design, vol. 27, no. 8, pp. 684–688, 2006.

[7] M. Rahimian, N. Ehsani, N. Parvin and H. Baharvandi, "The effect of particle size, sintering temperature and sintering time on the properties of Al–Al_2O_3 composites made by powder metallurgy", Journal of Materials Processing Technology, vol. 209, no. 14, pp. 5387–5393, 2009.

[8] S. M. Zebarjad and S.A. Sajjadi "Dependency of physical and mechanical properties of mechanical alloyed Al–Al_2O_3 composite on milling time," Materials and Design, vol. 28, no. 7, pp. 2113–2120, 2007.

[9] A. M. Al-Qutub, I. M. Allam and M. A. Abdul Samad, "Wear and friction of al–al_2o_3 composites at various sliding speeds," Journal of Materials Science, vol. 43, pp. 5797-5803, 2008.

[10] E. Ghasali, M. Alizadeh and T. Ebadzadeh, "Mechanical and microstructure comparison between microwave and spark plasma sintering of Al-B_4C composite," Journal of Alloys and Compounds, vol. 655, pp. 93-98, 2016.

[11] A. Nieto, H. Yang, L. Jiang and J. M. Schoenung, "Reinforcement size effects on the abrasive wear of boron carbide reinforced aluminum composites," Wear, vol. 390–391, pp. 228–235, 2017.

[12] K. Shirvanimoghaddam, H. Khayyam, H. Abdizadeh, M. Karbalaei Akbari, A. H. Pakseresht, E. Ghasali and M. Naebe, "Boron carbide reinforced aluminium matrix composite: physical, mechanical characterization and mathematical modelling," Materials Science & Engineering A, vol. 658, pp. 135-149, 2016.

[13] H. Guo and Z. Zhang, "Processing and strengthening mechanisms of boron carbide-reinforced aluminum matrix composites," Materials Today, vol. 73, no. 2, pp. 62-67, 2018.

[14] P. Li, E. G. Kandalova, V. I. Nikitin, A. G. Makarenko, A. R. Luts and Z. Yanfei, "Preparation of Al–TiC composites by self-propagating high-temperature synthesis, " Scripta Materialia, vol. 49, no. 7, pp. 699–703, 2003.

[15] A. R. Kennedy, D. P. Weston and M. I. Jones "Reaction in Al–Tic metal matrix composites" Materials Science and Engineering A, vol. 316, no. 1-2, pp. 32–38, 2001.

[16] A. E. Karantzalis, S. Wyatt and A. R. Kennedy, "The mechanical properties of Al-TiC metal matrix composites fabricated by a flux-casting technique," Materials Science and Engineering A, vol. 237, no. 2, pp. 200-206, 1997.

[17] S. Mohapatra, A. K. Chaubey, D. K. Mishra and S. K. Singh, "Fabrication of Al–TiC composites by hot consolidation technique: its microstructure and mechanical properties," Journal of Materials Research and Technology, vol. 5, no. 2, pp. 117–122, 2016.

[18] M. Ramachandra, A. Abhishek, P. Siddeshwar and V. Bharathi, "Hardness and wear resistance of ZrO_2 nano particle reinforced al nanocomposites produced by powder metallurgy," Procedia Materials Science, vol. 10, pp. 212-219, 2015.

[19] M. T. Abou El-Khair and A. Abdel Aal, "Erosion–corrosion and surface protection of A356 Al/ZrO_2 composites produced by vortex and squeeze casting," Materials Science and Engineering A, vol. 454–455, 156–163, 2007.

[20] W. Zhou, T. Yamaguchi, K. Kikuchi, N. Nomura and A. Kawasaki, "Effectively enhanced load transfer by interfacial reactions in multi-walled carbon nanotube reinforced Al matrix composites," Acta Materialia, vol. 125, pp. 369-376, 2017.

[21] H. M. Zakaria, "Microstructural and corrosion behavior of Al/SiC metal matrix composites", Ain Shams Engineering Journal, vol. 5, no. 3, pp. 831–838, 2014.

[22] Y. M. Han and X. G. Chen, "Electrochemical behavior of Al-B_4C metal matrix composites in NaCl solution," Materials, vol. 8, no. 9, pp. 6455-6470, 2015.

[23] S. F.Hassan, "Effect of primary processing techniques on the microstructure and mechanical properties of nano-Y_2O_3 reinforced magnesium nanocomposites," Materials Science and Engineering A, vol. 528, no. 16-17, pp. 5484–5490, 2011.

[24] O. R. Perez, S. Valdez, A. Molina, S. Mejia-Sintillo, C. Garcia-Perez, V. M. Salinas-Bravo and J. G.Gonzalez-Rodriguez, "Corrosion behavior of Al–Mg–Zn-Si alloy matrix composites reinforced with Y_2O_3 in 3.5% NaCl solution," International Journal of Electrochemical Science, vol. 12, pp. 7300-7311, 2017.

[25] F. Aydin and Y. Sun, "Investigation of wear behaviour and microstructure of hot-pressed TiB_2 particulate reinforced magnesium matrix composites," Canadian Metallurgical Quarterly, vol. 57, no. 4, pp. 455-469, 2018.

[26] F. Aydin, Y. Sun, M. E. Turan, "The effect of TiB_2 content on wear and mechanical behavior of AZ91 magnesium matrix composites produced by powder metallurgy," Powder Metallurgy and Metal Ceramics, vol. 57, pp. 564-572, 2019.

[27] M. R. Mattli, R. A. Shakoor, P. R. Matli, A. Mohamed and A. Mohamed, "Microstructure and compressive behavior of Al–Y_2O_3 nanocomposites prepared by microwave-assisted mechanical alloying," Metals, vol. 9, no. 4, pp. 1-9, 2019.

[28] F. Aydin and M. E. Turan, "The effect of boron nitride on tribological behavior of Mg matrix composite at room and elevated temperatures," Journal of Tribology, vol. 142, no. 1, pp. 1-7, 2020.

[29] I. Dinaharan and N. Murugan, "Dry sliding wear behavior of AA6061/ZrB_2 in-situ composite," Transactions Of Nonferrous Metals Society of China, vol. 22, no. 4, pp. 810-818, 2012.

[30] A. Standard, Standard practice for calculation of corrosion rates and related information from electrochemical measurements, Annu. Book Astm Stand. Astm Int.West Conshohocken Pa, 3 (2006) G102–G189.

[31] S. C. Sharma, "A study on stress corrosion behavior of Al6061/albite composite in higher temperature acidic medium using autoclave," Corrosion Science, vol. 43, no. 10, pp. 1877-1889, 2001.